RSC Advances

PAPER

View Article Online
View Journal | View Issue

Cite this: *RSC Adv.*, 2021, **11**, 22812

High-performance soy protein-based films from cellulose nanofibers and graphene oxide constructed synergistically *via* hydrogen and chemical bonding

Ningsi Wei, Murong Liao, Kaijie Xu and Zhiyong Qin *

Received 29th March 2021
Accepted 11th June 2021

DOI: 10.1039/d1ra02484a

rsc.li/rsc-advances

Soybean protein isolate (SPI) shows a broad application prospect in the food and packaging industry. However, its inferior mechanical properties and water resistance limit its application. In this work, a series of SPI-based composite films were prepared by combining with cellulose nanofiber (CNF), graphene oxide (GO), GO/CNF, ethylene glycol diglycidyl ether (EDGE) or GO/CNF/EGDE. The results show that by adding a small amount of reinforced materials (3%), the water resistance, hydrophilicity, mechanical properties and thermal stability of composite films were improved. The filling effect and hydrogen bonding of the reinforcing materials contribute to the formation of film structure. EGDE cross-link SPI with CNF and GO build a chemical network to improve the properties of the film. In addition, they could make a synergistic effect to better enhance the performance of a protein film. Therefore, the tensile strength and elastic modulus of the SGCE film reached 469.21% and 367.58%, respectively.

1. Introduction

The depletion of petroleum resources and the "white pollution" caused by synthetic polymers make researchers turn their attention to biomass materials, which are a wide variety of sources, biodegradable, renewable and environmentally friendly.[1,2] The packing film constructed by biomass could be an ideal substitute for petroleum-based packaging materials because it contains excellent barrier performance, which can prevent water vapor, O_2 and CO_2 from passing through to keep the food fresh.[3] As a part of biomass materials, proteins have the same advantages. Among protein, soybean protein isolate (SPI) can be accessed from soybeans and is a by-product of soy oil processing that makes it become a potential replacement in packing materials.[4] SPI contains great film-forming performance, a SPI-based film could be formed after adding a small amount of plasticizer. However, the SPI film also has disadvantages such as low strength, poor water resistance and barrier performance, so it needs to be further modified to meet the practical requirements. The performance of the SPI film is influenced a lot by the non-covalent forces (hydrophobic interactions, hydrogen bonding, and electrostatic attractions), and it could be modified by physical,[5,6] chemical[7] or biological methods to produce new packing materials with excellent properties.

Various approaches, including molecular modification, ultrasound modification, high-pressure homogenization, filling of nanoparticles and adding crosslinking agents, have been applied to enhance the properties of soy protein materials. By ultrasound modification, the chemical bonds of SPI molecules were broken, exposing more active groups, increasing cross-linking entanglement and improving the tensile properties. The mechanism could change the structural and functional properties by high energy impact, which reduces the particle size, increases surface hydrophobicity of SPI and forms soluble aggregates, leading to a denser and more uniform polymer networks.[8–11] Nevertheless, the high-cost equipment and poor mechanical performance of conventional physical modification are driving the research community to seek more efficient and sustainable alternatives. Epoxy crosslinking is a good choice for improving the mechanical properties of SPI composites. The epoxy cross-linker agent is prone to ring-opening polymerization and forms a more stable chemical structure with soybean protein owing to many polar functional groups, such as –OH, $–NH_2$, –COOH, and –SH.[11] For instance, as a commonly used epoxy-crosslinking agent, EGDE can react with protein molecules by its epoxy-functional groups.[12]

In recent years, growing interest has been devoted to functional nanomaterial mainly due to their characteristic of large specific surface area, high surface activity and the small size effect. Such materials play an important role in the fields of biology,[13] energy conversion,[14] catalysis,[15] and chemical sensors.[16] Adding inorganic nanoparticles such as montmorillonite,[17–20] halloysite nanotubes,[21,22] silica,[23] carbon nanotubes,[24] and graphene oxide[25–27] can effectively improve the mechanical properties, barrier properties and heat resistance of the composite film.

Guangxi University, School of Resources, Environment and Materials, Nanning 530000, China. E-mail: qinzhiyong@gxu.edu.cn

Han[6] mixed different sizes of SiO_2 nanoparticles with the SPI film and found that the water content and soluble total matter content of the composite film decreased with decreasing size of SiO_2, and the addition of SiO_2 improved the thermal stability of the film. Kang[28] used dopamine for surface modification of halloysite nanotubes (HNTs) and then grafted the silane agent. Finally, a PDHNTs/SPI film was obtained after mixing SPI with the modification HNTs, its tensile strength increased from 5.90 MPa to 8.73 MPa and Young's modulus improved by 54.5%. There are reports that the mechanical properties of composites have been remarkably improved including tensile strength (up to 280.70%) and toughness (up to 258.30%), because of the efficient dissipation mechanisms derived from the synergistic interfacial interactions between the GO load distribution and SPI matrix.[29] However, many reports show that graphene contains a large number of active groups and is easy to agglomerate in composites.[30] CNF is often used as a dispersing agent to disperse nanoparticles because of their large specific surface area and good dispersion. Because of the physical cross-linking and strong hydrogen bond association between CNF and polymers, it is very obvious for CNF to reinforce polymers in terms of mechanical properties and barrier properties.[31–34] Therefore, it has great potential for doping with GO and CNF to prepare inorganic–organic composites.

Herein, in a facile strategy, CNF and GO were selected as fillers to prepare SPI-based composite films with excellent mechanical properties by ultrasonic dispersion and EGDE cross-linking was proposed. A series of SPI-based composite films were produced by the solution casting method. Then, a small quantity of reinforcement (3%) or cross-linking agent was loaded into the matrix; the effects of incorporating CNF, GO and EGDE on surface compositions, microstructure and thermal properties of the films were investigated, and the reaction mechanism was also proposed. In addition, the mechanical, total solubility and contact angle of composite films are discussed.

2. Materials and methods

2.1 Materials

SPI with a protein content of over 95% was purchased from Shandong Yuwang Ecological Food Industry Co., Ltd. Glycerol of biotechnology grade (Shandong, China). EGDE was purchased from McLean Biochemical Reagent Co., Ltd (Shanghai, China). CNF was provided by a modified technical scheme, its diameter and length were 4–10 nm and 1000–3000 nm, respectively.[35] GO powder was synthesized by a modified Hummers' method according to a previously published method.[30] Sodium hydroxide (NaOH) solution (10%, w/w) was prepared from NaOH solid powder (≥97%, Kelon Chemical Reagent Factory, Chengdu, China). All chemicals were used without further purification.

2.2 Preparation of SPI-based composite film

2 g of SPI powders and 0.6 g of glycerol were dissolved in 38 ml deionized water to prepare SPI suspension, and its pH was adjusted to 9.0 ± 0.2 using 10% NaOH solution (w/w). The suspension was agitated for 30 min at 80 °C to disrupt the peptide chain structure of protein and cause the partial denaturation of protein. CNF or GO was dispersed in deionized water and treated under sonication at 400 W for 10 min to form a homogeneous 0.5% (w/w) solution. After that, the CNF solution, GO solution and EGDE were added into the SPI suspension, stirring for 10 min and were treated with ultrasound to obtain a series of film-forming solutions. Finally, the mixed solution was poured in plastic Petri dishes and water was evaporated in a temperature humidity chamber at 45 °C and 45 RH% for 24 h. All the prepared samples were conditioned in a dryer at 57 ± 2RH% and 25 ± 2 °C for 3 days before testing (Table 1).

2.3 Characterization

2.3.1 Mechanical properties. A handheld digital micrometer (Measuring & Cutting Tool Co., Ltd. Guilin, China) with a sensitivity of 0.001 mm was utilized to measure the dimension of each film. Then, the mechanical properties were performed according to the ASTM D880-02 standard. Specimens (10 mm × 60 mm) were tested using a universal tensile testing machine (AG-X Plus, Shimadzu Corporation, Japan) with a strain rate of 50 mm min^{-1} and a gauge length of 30 mm. Young's modulus, tensile strength and fracture strain were measured from the tests.[29]

2.3.2 Total soluble matter (TSM). The TSM of SPI-based composite films was measured according to a method described by Xu *et al.*[36]. First, all specimens were dried in an air-circulating oven at 103 ± 2 °C to water eliminate the free water and reached a constant weight, weighing (m_1). Then, the specimens were placed in distillation bottles containing distilled water, magnetically stirring every 2 h for 24 h at room temperature (25 ± 2 °C). Finally, all specimens were taken out and dried under the same drying condition in an air-circulating oven, until they reached a constant weight again, weighing (m_2). The TSM of SPI-based composite sheets was calculated as follows:

$$\mathrm{TSM}\ (\%) = (m_1 - m_2)/m_1 \times 100$$

2.3.3 Surface contact angle (CA). The CA tests on the specimens were conducted on a DSA100 contact angle meter (KRUSS Co., Ltd. Hamburg, Germany) at room temperature. Each specimen was cut to a size of 20 mm × 80 mm and fixed

Table 1 Code and formulation of SPI-based composite films[a]

Samples	SPI (g)	Glycerol (g)	CNF (g)	GO (g)	EGDE (g)
SPI	2	0.6	—	—	—
SC	2	0.6	0.06	—	—
SG	2	0.6	—	0.06	—
SE	2	0.6	—	—	0.2
SCG	2	0.6	0.03	0.03	—
SCGE	2	0.6	0.03	0.03	0.2

[a] All components were added relative to the content of SPI.

on a slide horizontally using a double-sided adhesive. Then, 5 μL water droplets were dropped on the surface of the specimen by a digital micro-syringe. Finally, the result was obtained after six parallel measurements.

2.3.4 Fourier transform infrared spectroscopy analysis (FTIR). The FTIR spectra of SPI-based films were obtained using a spectrometer (Nicolet 7600 Nico-let Instrument Corporation, Madison, WI, USA) with an average of 32 scans recorded from 400 to 4000 cm^{-1} wavenumbers at a resolution of 4 cm^{-1}.

2.3.5 X-ray diffraction (XRD). X-ray diffraction patterns of SPI-based composite films were investigated on an X-ray diffractometer (MINFLEX600, science company Co., Ltd, Shanghai, China) equipped with Cu Kα1 radiation at 40 kV and 40 mA. Data were collected at a 2° min^{-1} scan rate from 5° to 60° Bragg angle (2θ).

2.3.6 Differential-scanning calorimeter (DSC). The thermal transition characteristic of SPI-based composite films was carried out on Polyma DSC-214 (NETZSCH, Germany). About 4–5 mg of the specimen was compressed in aluminum standard pans and tested in the range from room temperature to 250 °C at a rate of 10 °C min^{-1}.

2.3.7 Thermogravimetric analysis (TGA). The thermal stability characteristic of each film was investigated using thermogravimetric analysis (TGA, Q50, TA Instruments, MA, USA). The specimens were dried in a desiccator with P_2O_5 at room temperature to receive a constant weight. After that, each specimen was placed in a platinum cup at a flow of 60 ml min^{-1} nitrogen gas and heated to 600 °C at a heating rate of 10 °C min^{-1}. The peak temperature at the maximum degradation rate was calculated.

2.3.8 Scanning electron microscopy (SEM). SEM analysis was performed using scanning electron microscopy (ZEISS, Germany) at an acceleration voltage of 15 kV. In order to receive distinct images of the cross-sectional fracture surface morphologies of the SPI-based composite films, the cross-sectional fracture was first sputter-coated with a gold layer and then observed.

3. Results and discussion

3.1 Physical and mechanical properties of SPI-based composite films

The physical and mechanical properties of SPI composite films are important factors for applications. The effect of the different components on the mechanical properties of SPI film was studied and the results are shown in Fig. 1(a–c), and the specific data are illustrated in Table 2. In this study, the mechanical strength of the pure SPI film was only 3.28 MPa, similar to that prepared by other researchers.[29,37] Compared to the pure film, the tensile strength and Young's modulus of SG and SC films were improved to some extent. It was probably attributed to the reinforcement of GO or CNF and interfacial interaction between them and SPI. GO or CNF could effectively fill the internal void in the SPI-based film and form a significant physical network

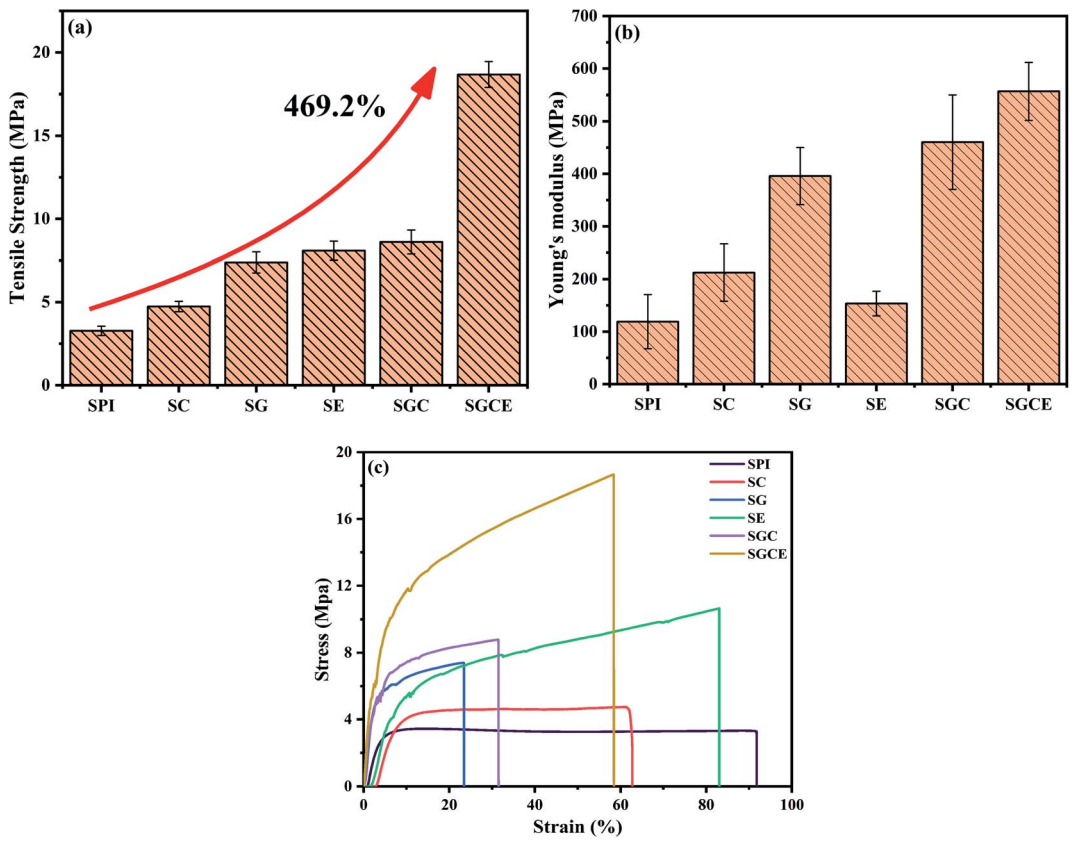

Fig. 1 Mechanical tensile testing of SPI-based composite films: (a) the tensile strength (b) Young's modulus and (c) tensile curves.

Table 2 The effect of different components to the mechanical properties of SPI-based composite film[a]

Sample	TS (MPa)	EB (MPa)	*E* (%)
SPI	3.28 ± 0.28	119.06 ± 51.65	91.26 ± 17.53
SC	4.74 ± 0.63	212.41 ± 30.95	64.62 ± 10.69
SG	7.39 ± 0.63	395.95 ± 54.40	22.38 ± 375
SE	8.09 ± 0.57	153.55 ± 23.45	82.51 ± 9.32
SGC	8.61 ± 0.72	460.38 ± 90.02	13.38 ± 5.52
SGCE	18.67 ± 0.57	556.70 ± 54.94	55.57 ± 4.71

[a] TS: tensile strength, EB: elongation at break, *E*: elastic modulus.

with SPI molecules through the active functional groups on the surface of them. The SG film has better mechanical properties than those of the SC film because the surface of GO contained abundant oxygen-containing groups, which can form more stable chemical bonds by reaction between oxygen groups and hydroxyl or amino groups on protein molecules. The mechanical properties of the SE film also increased, resulting from the ring-opening reaction between epoxy groups of EGDE and amino groups (or hydroxyl) of SPI.[12] By this reaction, a cross-linked network was constructed and led the SPI-based composite film to become more compact.

When CNF and GO were added to the matrix together, a significant change was observed in mechanical properties, and the tensile strength and Young's modulus of the SGC film was increased by 162.50%, 286.68%, respectively. This could be attributed to the synergistic effect of reinforcing agents; single component doping has a limited reinforcing effect, and the synergistic reinforcing effect of doping with various substances was of great significance to composites.[23,38] The tensile strength and Young's modulus of the SGCE film leaped by 469.21%, 397.58%, respectively. It may because of the synergistic effect of physical entanglement, non-covalent interactions and chemical crosslink. A continuous network was constructed through hydrogen bonds between GO, CNF and SPI, as well as EGDE could interact with active groups on the surface of SPI and nanoparticles to build a dense crosslinking network, as shown in Fig. 2. The structure and properties of the SGCE film have been greatly enhanced, which provided an effective reference for the future application and design of SPI composite materials.

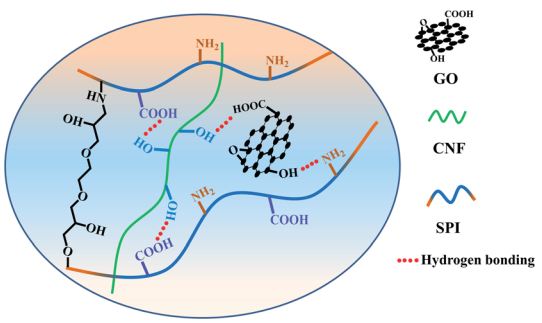

Fig. 2 Proposed synergistic mechanism in SPI-based composite films.

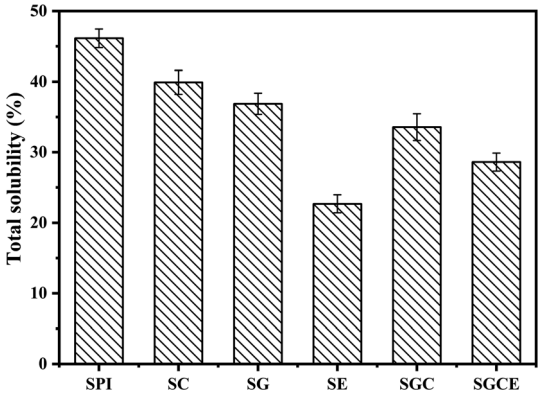

Fig. 3 The total solubility of the SPI-based composite films.

3.2 Water resistance properties of SPI-based composite films

The water resistance of the SPI-based composite films is displayed in Fig. 3. In addition, the TSM of the original SPI film was 46.14%, consistent with previous reports.[39] The dissolved matter of SG, SC, SE, SGC and SGCE composite films decreased by 19.87%, 13.50%, 50.80%, 27.20% and 38.01%, respectively, relative to that of the pure protein film. It is shown that the water-resistance of SPI-based composite films was significantly improved after adding nanoparticles or the cross-linking agent. Similar to previous mechanical properties, the modification of CNF, GO and EGDE may greatly promote the generation of cross-linked polymer networks of SPI molecules, thus reducing water penetration into the films.

The water contact angle is an important index to evaluate the water sensitivity of the SPI-based composite films. Generally, the larger the contact angle on the surface of the composite film, the stronger is its hydrophobicity, and *vice versa*. The CA of the SPI-based composite films is shown in Fig. 4. In this study, the CA of pure protein film is 62.10°, illustrating its hydrophilic. After adding CNF or GO to the matrix, the CAs of SC, SG and SCG films were 58.33°, 44.0°, 54.77° respectively, both CA of them has been reduced. The CA of SG film is lowest because the surface of GO contains more polar groups that could effectively improve the hydrophilicity of the composite film. The CA of the SE film was 51.26°, suggesting that crosslinking would create a smooth and compact surface resulting in the decrease of the CA. This can be proved by the results of SEM. All the components added to the matrix show the effect of reducing the CA of the SPI film, therefore, the CA of the SCGE film was 45.85 which is smaller than that of the pure SPI film.

3.3 Chemical structural analysis of SPI-based composite films

To investigate the interaction of different SPI-based composite films, FTIR was performed, and the result is illustrated in Fig. 5(a). The characteristic spectrum of the SPI-based composite films exhibited typical absorption bands related to proteins, such as (i) amide I (C–O stretching at 1633 cm^{-1}); (ii) amide II (N–H bending vibration at 1535 cm^{-1})[40] and (iii) amide III (combined C–N stretching and N–H bending vibrations

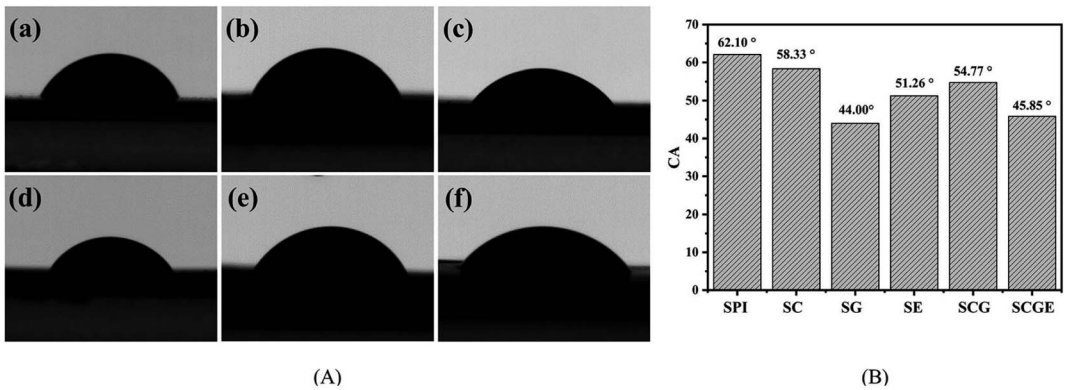

Fig. 4 The images of contact angle of SPI-based composite films. (A) Contact angle of SPI-based composite films. (B) Contact angle data of SPI-based composite films.

between 1470 cm^{-1} and 1314 cm^{-1}).[41,42] It could be clearly seen that the C–O stretching band at 1159 cm^{-1} of SE and SGCE film disappeared, due to the ring-opening reaction, indicating that CNF and GO were successfully incorporated into the SPI matrix.[29,43]

Changes in the peak intensity in the region related to amide III (better identified at 1400 cm^{-1}) were noticeable, indicating that the main chain amide formed a connection with the carboxyl group of the cellulose chain or the oxygen group on GO. The formation of these bonds can explain the reasons for the high stiffness and low water solubility of the film after adding GO and CNF.

The crystal structure and compatibility of film samples were observed by analyzing the XRD patterns shown in Fig. 5(b). Two characteristic crystallization diffraction peaks at 8.8° and 19.8° corresponded to α-helix and β-sheet structures, respectively, of the secondary structure of SPI.[44] For patterns of SC and SGC films, a sharp characteristic peak appeared at 22.6° related to the crystal of cellulose I, indicating that CNF was successfully added to the SPI matrix and exhibited great compatibility. In addition, above the patterns of SE and SGCE films, the peak of $2\theta = 9.8°$ becomes smooth that may because the ring-opening reaction occurs between EGDE and SPI, which can change the crystal lattice of the α-helix belongs to SPI.

3.4 Thermal performance analysis of SPI-based composite films

DSC is mainly used to characterize the thermal behavior of substances. The DSC curves of SPI composite films are shown in Fig. 6(a). There were typical melting endothermic peaks of polymers in each sample. Evidently, the endothermic peak of pure protein film was at 124.8 °C. In the SG film and SGC film with GO added, the T_m migrated to low temperature. It was because of the physical partition of protein molecular chains by GO intercalation, which enhanced the mobility and flexibility of protein molecular chains, thus reducing the melting temperature. On the contrary, owing to the CNF adding, protein molecular chains and CNF entangling, the fluidity of protein molecular chains was reduced. Interestingly, due to the synergistic enhancement of GO, CNF and EGDE, the more complex entanglement crosslinking made T_m of the SGCE film being significantly enhanced.

The mass loss traces of SPI-based films (TGA curves) are revealed in the temperature range from room temperature up to 600 °C Fig. 6(b). Thermal degradation of all SPI films consisted of three stages. Weight loss in the first stage (below 100 °C) was assigned to the evaporation of residual moisture. The evaporation of glycerol and the thermal degradation of proteins were included, which results in the weight loss between 100 and 220 °C, as well as between 250 and 450 °C. It can be seen from

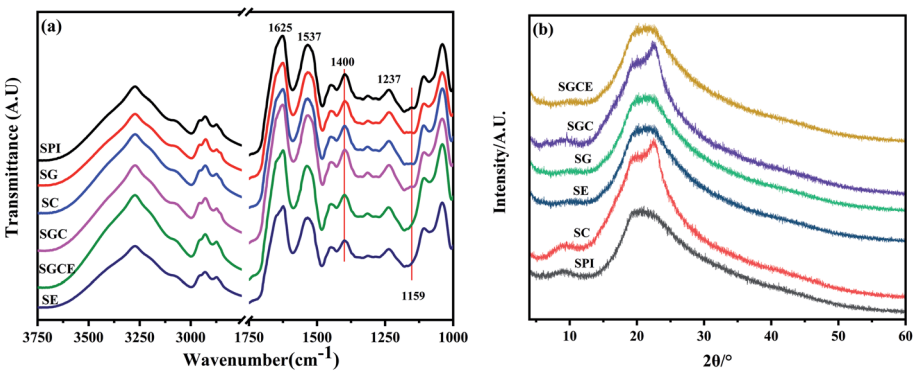

Fig. 5 Chemical structural analysis of the SPI-based composite films: (a) FTIR spectra and (b) XRD patterns.

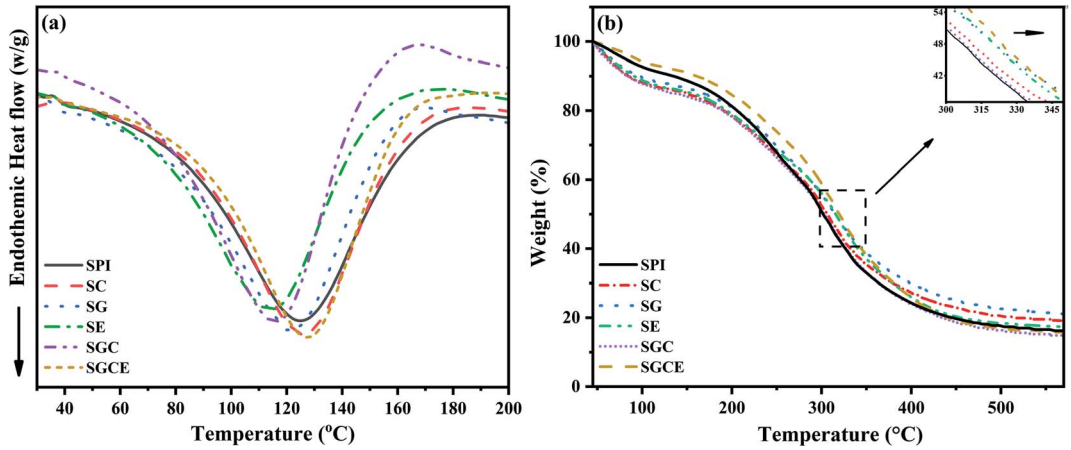

Fig. 6 The performance and behavior of thermal of SPI-based composite films: (a) DSC curves and (b) TGA curves.

Table 3 Thermal parameters of soybean protein isolate composite films[a]

Samples	SPI	SG	SC	SE	SGC	SGCE
T_g (°C)	76.1	76.0	66.2	86.0	75.5	90.0
T_m (°C)	124.8	120.7	126.4	114.1	115.6	128.2
T_{Max} (°C)	311.5	315.3	314.7	319.3	319.6	322.0

[a] T_g: temperature of glass transition, T_m: temperature of melting, T_{Max}: temperature of maximum decomposition rate of protein.

Fig. 6(b) that, compared with pure SPI film, the TG curves of all SPI-basic composite films deviated at the maximum decomposition temperature of the protein, indicating that the thermal stability of composite films was improved. As shown in Table 2, with the addition of fillers, the temperature of the maximum decomposition rate of the composite films rose from 311.5 °C to 322 °C, which was related to the crosslinking and interfacial interaction between the fillers, crosslinking agents and protein molecules that could effectively improve the thermal stability of the SPI-based films.

The temperature of glass transition (T_g) is an important physical property of amorphous polymers. Table 3 reveals that the T_g of the original SPI was 76.1 °C and the addition of GO had no effect on the T_g of the SG film. The addition of CNF enlarged the amorphous region of SPI and decreased the T_g of the SC film compared to that of the pristine SPI. Similarly, the addition of GO and CNF also decreased the T_g of SGC film, not by as much as SC film. The possible reason was that CNF has a hydrogen bond with GO, which made the SGC film more uniform and orderly than the SC film. Further, with EGDE adding, the composite film became more compact and orderly. As the result shows, the T_g of SGCE film went up to 90 °C, which strongly implied that the CNF/GO/EGDE synergistically enhanced the SPI film.

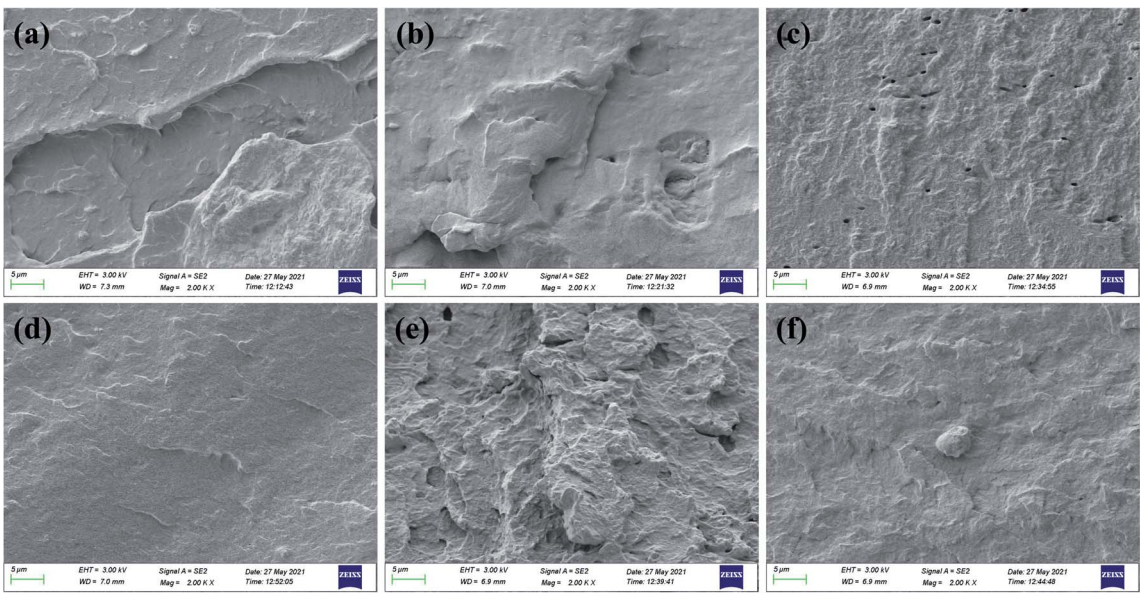

Fig. 7 Cross-sectional SEM images of SPI-based composite films: (a) SPI, (b) SC, (c) SG, (d) SE, (e) SCG, and (f) SCGE.

3.5 Micromorphology

The cross-sectional morphology of SPI-based composite films was examined by SEM. Fig. 7(a) shows the cross-section of the original SPI film was smooth, continuous, and uniform due to the relatively low physical crosslinking degree of the protein (3.28 MPa). As shown in Fig. 7(b and c), when CNF or GO was added the matrix, the SC film shows a relatively smooth and continuous surface, while the SEM image of SG film is rough and displays many holes. This suggested that CNF dispersed well in the composite film and promoted the formation of a dense and continuous surface; GO relative to its poor dispersion led to the brittle fracture of the SG film (22.38 ± 3.75). The cross-section of the SGC film is very rough and has obvious protrusions corresponding to a larger cross-sectional area, which plays a role in mechanical enhancement. As presented in Fig. 7(d and e), the cross-sectional structures in SE and SCGE film are somewhat similar, they both display some folds and strip-shaped bulges, indicating that the cross-linking of EGDE can produce a continuous and homogenous film structure, resulting in the improvement of mechanical properties.[7] Moreover, the SCGE film has more roughness cross-section suggesting the chemical cross-linking and hydrogen bonding between CNF, GO, EGDE and protein molecules significantly increasing the entanglement and crosslinking of the composite film. Then, resulting in sustaining more energy in the process of stress breakage, in accordance with the previous studies, the SGCE film showed strong mechanical properties that are similar to previous studies.

4. Conclusions

In this work, an excellent performance SPI-based film was successfully fabricated *via* a facile approach by incorporating CNF, GO and EGDE. This study illustrated that the addition of CNF, GO and EGDE effectively enhanced the properties of the composite film. Compared to the pure SPI film, the tensile strength of the SGCE film increased by 469.21%. It indicated that the fill effect, hydrogen bonding and chemical crosslinking synergistically play a major role in energy dissipation during tensile failure of the composite film. Moreover, the decrease in TSM and CA was noticed, it was attributed to filler and cross-linking agent added to the matrix, effectively enhancing the surface polarity of the composite film. FTIR and XRD results demonstrated that the strong hydrogen bond formed between hydroxyl with amino groups; meanwhile, the ring-opening polymerization occurred between the epoxy group and amino groups. These findings indicated that the SGCE film with high strength may have great potential in the packaging field, which provides hope for green materials and accelerates the development of energy-efficient utilization.

Conflicts of interest

The authors declare that they have no known competing financial interests or personal relationships that could have appeared to influence the work reported in this paper.

Acknowledgements

This research was supported by the Fundamental Research Funds for the National Natural Science Foundation of China (Project 31790188), and the Innovation-Driven Project Funds of Guangxi (AA17204087-15).

References

1 A. K. Mohanty, S. Vivekanandhan, J.-M. Pin and M. Misra, *Science*, 2018, **362**, 536.
2 H. Hu, J. Wu, E. C. Y. Li-Chan, L. Zhu, F. Zhang, X. Xu, G. Fan, L. Wang, X. Huang and S. Pan, *Food Hydrocolloids*, 2013, **30**, 647–655.
3 Y. Xiao, Y. Liu, S. Kang, K. Wang and H. Xu, *Food Hydrocolloids*, 2020, **106**, 105898.
4 P. Guerrero, T. Garrido, I. Leceta and K. de la Caba, *Eur. Polym. J.*, 2013, **49**, 3713–3721.
5 J. Wu, Q. Sun, H. Huang, Y. Duan, G. Xiao and T. Le, *Clin. Chim. Acta*, 2019, **180**, 31–38.
6 Y. Han and L. Wang, *RSC Adv.*, 2016, **6**, 112317–112324.
7 T. Li, N. Xia, L. Xu, H. Zhang, H. Zhang, Y. Chi, Y. Zhang, L. Li and H. Li, *Food Packag. Shelf Life*, 2021, **27**, 100614.
8 H. Hu, E. C. Y. Li-Chan, L. Wan, M. Tian and S. Pan, *Food Hydrocolloids*, 2013, **32**, 303–311.
9 R. Morales, K. D. Martínez, V. M. Pizones Ruiz-Henestrosa and A. M. R. Pilosof, *Ultrason. Sonochem.*, 2015, **26**, 48–55.
10 Z. Wang, N. Zhang, H.-y. Wang, S.-y. Sui, X.-x. Sun and Z.-s. Ma, *LWT–Food Sci. Technol.*, 2014, **57**, 548–555.
11 F. Song, D.-L. Tang, X.-L. Wang and Y.-Z. Wang, *Biomacromolecules*, 2011, **12**, 3369–3380.
12 Y. Zhao, M. He, H. Jin, L. Zhao, Q. Du, H. Deng, W. Tian, Y. Li, X. Lv and Y. Chen, *Chem. Eng. J.*, 2018, **341**, 402–413.
13 J. Ren, R. Cai, J. Wang, M. Daniyal, D. Baimanov, Y. Liu, D. Yin, Y. Liu, Q. Miao, Y. Zhao and C. Chen, *Nano Lett.*, 2019, **19**, 4692–4701.
14 V. Chikan and D. F. Kelley, *Nano Lett.*, 2002, **2**, 141–145.
15 K. V. Karthik, C. V. Reddy, K. R. Reddy, R. Ravishankar, G. Sanjeev, R. V. Kulkarni, N. P. Shetti and A. V. Raghu, *J. Mater. Sci.: Mater. Electron.*, 2019, **30**, 20646–20653.
16 Z. Xu, Y. Luo and G. Duan, *ACS Appl. Mater. Interfaces*, 2019, **11**, 8164–8174.
17 I. Echeverría, P. Eisenberg and A. N. Mauri, *J. Membr. Sci.*, 2014, **449**, 15–26.
18 P. Kumar, K. P. Sandeep, S. Alavi, V. D. Truong and R. E. Gorga, *J. Food Sci.*, 2010, **75**, N46–N56.
19 P. Kumar, K. P. Sandeep, S. Alavi, V. D. Truong and R. E. Gorga, *J. Food Eng.*, 2010, **100**, 480–489.
20 H. Wang, H. Zhang, B. Niu, S. Jiang, J. Cheng and S. Jiang, *RSC Adv.*, 2016, **6**, 29294–29302.
21 H. Kang, Z. Wang, S. Zhao, Q. Wang and S. Zhang, *J. Appl. Polym. Sci.*, 2018, **135**, 46197.
22 X. Liu, R. Song, W. Zhang, C. Qi, S. Zhang and J. Li, *Sci. Rep.*, 2017, **7**, 44289.
23 D. E. Coupry, J. Butson, P. S. Petkov, M. Saunders, K. O'Donnell, H. Kim, C. Buckley, M. Addicoat, T. Heine and P. Á. Szilágyi, *Chem. Commun.*, 2016, **52**, 5175–5178.

24 Q. Meng and I. Manas-Zloczower, *Compos. Sci. Technol.*, 2015, **120**, 1–8.
25 J. Jose, M. A. Al-Harthi, M. A.-A. AlMa'adeed, J. Bhadra Dakua and S. K. De, *J. Appl. Polym. Sci.*, 2015, **132**, 41827.
26 H.-K. Seo, M.-H. Park, Y.-H. Kim, S.-J. Kwon, S.-H. Jeong and T.-W. Lee, *ACS Appl. Mater. Interfaces*, 2016, **8**, 14725–14731.
27 S. Xia, L. Yao, Y. Zhao, N. Li and Y. Zheng, *Chem. Eng. J.*, 2015, **280**, 720–727.
28 H. Kang, X. Liu, S. Zhang and J. Li, *RSC Adv.*, 2017, **7**, 24140–24148.
29 Z. Wang, H. Kang, S. Zhao, W. Zhang, S. Zhang and J. Li, *Carbohydr. Polym.*, 2018, **180**, 354–364.
30 T. B. Rouf and J. L. Kokini, *J. Mater. Sci.*, 2016, **51**, 9915–9945.
31 Q. Fang, M. Zhu, S. Yu, G. Sui and X. Yang, *J. Mater. Sci. Eng. B*, 2016, **214**, 1–10.
32 K.-Y. Lee, Y. Aitomäki, L. A. Berglund, K. Oksman and A. Bismarck, *Compos. Sci. Technol.*, 2014, **105**, 15–27.
33 M. B. K. Niazi, Z. Jahan, S. S. Berg and Ø. W. Gregersen, *Carbohydr. Polym.*, 2017, **177**, 258–268.
34 D. M. Panaitescu, A. N. Frone, M. Ghiurea and I. Chiulan, *Ind. Crops Prod.*, 2015, **70**, 170–177.
35 S. Wang, C. Wei, Y. Gong, J. Lv, C. Yu and J. Yu, *RSC Adv.*, 2016, **6**, 10168–10174.
36 F. Xu, Y. Dong, W. Zhang, S. Zhang, L. Li and J. Li, *Ind. Crops Prod.*, 2015, **67**, 373–380.
37 S. Zhang, C. Xia, Y. Dong, Y. Yan, J. Li, S. Q. Shi and L. Cai, *Ind. Crops Prod.*, 2016, **80**, 207–213.
38 S.-J. Chun, S.-Y. Lee, G.-H. Doh, S. Lee and J. H. Kim, *J. Ind. Eng. Chem.*, 2011, **17**, 521–526.
39 Z. Qin, L. Mo, M. Liao, H. He and J. Sun, *Polymers*, 2019, **11**, 1185.
40 A. Barth, *Biochim. Biophys. Acta, Bioenerg.*, 2007, **1767**, 1073–1101.
41 M. Božič, M. Majerič, M. Denac and V. Kokol, *J. Appl. Polym. Sci.*, 2015, **132**, 41837.
42 P. Guerrero, J. P. Kerry and K. de la Caba, *Carbohydr. Polym.*, 2014, **111**, 598–605.
43 D. Xu, J. Zhang, Y. Cao, J. Wang and J. Xiao, *LWT–Food Sci. Technol.*, 2016, **66**, 590–597.
44 J.-F. Su, Z. Huang, Y.-H. Zhao, X.-Y. Yuan, X.-Y. Wang and M. Li, *Ind. Crops Prod.*, 2010, **31**, 266–276.